Journal of Materials Chemistry B

ROYAL SOCIETY OF CHEMISTRY

PAPER

View Article Online
View Journal | View Issue



Cite this: J. Mater. Chem. B, 2024, 12, 5535

# Investigation of a chondroitin sulfate-based bioactive coating for neural interface applications†

Vaishnavi Dhawan, [ab] Paige Nicole Martin, [a] Xiaoming Hu[c] and Xinyan Tracy Cui *[ab]

Invasive neural implants allow for high-resolution bidirectional communication with the nervous tissue and have demonstrated the ability to record neural activity, stimulate neurons, and sense neurochemical species with high spatial selectivity and resolution. However, upon implantation, they are exposed to a foreign body response which can disrupt the seamless integration of the device with the native tissue and lead to deterioration in device functionality for chronic implantation. Modifying the device surface by incorporating bioactive coatings has been a promising approach to camouflage the device and improve integration while maintaining device performance. In this work, we explored the novel application of a chondroitin sulfate (CS) based hydrophilic coating, with anti-fouling and neurite-growth promoting properties for neural recording electrodes. CS-coated samples exhibited significantly reduced protein-fouling *in vitro* which was maintained for up to 4-weeks. Cell culture studies revealed a significant increase in neurite attachment and outgrowth and a significant decrease in microglia attachment and activation for the CS group as compared to the control. After 1-week of *in vivo* implantation in the mouse cortex, the coated probes demonstrated significantly lower biofouling as compared to uncoated controls. Like the *in vitro* results, increased neuronal population (neuronal nuclei and neurofilament) and decreased microglial activation were observed. To assess the coating's effect on the recording performance of silicon microelectrodes, we implanted coated and uncoated electrodes in the mouse striatum for 1 week and performed impedance and recording measurements. We observed significantly lower impedance in the coated group, likely due to the increased wettability of the coated surface. The peak-to-peak amplitude and the noise floor levels were both lower in the CS group compared to the controls, which led to a comparable signal-to-noise ratio between the two groups. The overall single unit yield (% channels recording a single unit) was 74% for the CS and 67% for the control group on day 1. Taken together, this study demonstrates the effectiveness of the polysaccharide-based coating in reducing biofouling and improving biocompatibility for neural electrode devices.



Received 8th March 2024,
Accepted 9th May 2024

DOI: 10.1039/d4tb00501e

rsc.li/materials-b

## 1. Introduction

Advancements in neural prostheses have enabled the treatment of neurological disorders, spinal cord injuries, and stroke to assist patients in regaining function. For such neuroprosthetic applications and brain–computer-interface technologies (BCI), neural interfaces are integral for facilitating the stimulation of neurons and recording neural activity.[1]

Specifically, intracortical recording electrodes are utilized for their increased capacity to record single-unit (SU) action potentials and local field potentials (LFPs).[2] However, the mechanical insertion of these probes is inherently traumatic and evokes an immune response. The tearing of blood vessels releases serum proteins which can non-specifically adsorb on the device surface and can have an acute pro-inflammatory and neurotoxic effect.[3,4] Meanwhile, insertion trauma causes the activation of resident microglia, which extend their processes toward the device beginning to encapsulate it.[5,6] A subsequent inflammatory cascade is triggered which can lead to a chronic glial sheath formation around the implant barring signal transmission, along with demyelination and neuronal degeneration.[3,7] A combination of loss of neurons and glial encapsulation can contribute to low acute recording yield and

[a] Department of Bioengineering, University of Pittsburgh, Pittsburgh, PA, USA. E-mail: xic11@pitt.edu
[b] Center for Neural Basis of Cognition, Pittsburgh, PA, USA
[c] Department of Neurology, University of Pittsburgh, PA, USA

† Electronic supplementary information (ESI) available. See DOI: https://doi.org/10.1039/d4tb00501e

deterioration of recording quality for chronic electrode implants.[8]

Modifying the implant surface with hydrophilic synthetic coatings, such as zwitterionic polymers, can help to reduce the non-specific protein fouling upon implantation. In doing so, the extent of acute inflammation around the implant site can be dampened, prolonging device function *in vivo*.[9–12] However, due to the synthetic nature of the material, seamless integration with the tissue is limited. Biomimetic or bioactive coatings can address this limitation by interacting with the tissue to promote integration and improve device biocompatibility.[13] A prominent approach is to promote neurite attachment by utilizing transmembrane proteins as coatings, such as N-cadherin and neuronal cell adhesion molecule L1.[14–16] Specifically, L1 was shown to increase neuronal density and reduced glial encapsulation around the coating, and demonstrated enhanced recording quality for a chronic 16-week implantation.[16–18] Protein-based coatings can be fragile and may be subject to degradation during coating fabrication and long-term application. While our group has developed a nanoparticle-based coating that can stabilize the protein without losing bioactivity for 28 days in storage,[18] this additional step does extend the processing pipeline for the coating.

While new strategies exploring polymer-enabled bioactive coatings are being actively investigated, the use of carbohydrate-based coatings has been mostly unexplored for neural interface applications. Carbohydrates, in their linear or branched polysaccharide form, are attached to lipids and cell membrane protein anchors and play a critical role in neural development.[19–25] Chondroitin sulfate proteoglycans (CSPGs) are a type of glycoconjugate composed of alternating disaccharide units of *N*-acetylgalactosamine (GalNAc) and glucuronic acid (GlcA) attached to a protein core that tethers it to the extracellular matrix (ECM).[26,27] There are differential sulfation patterns on the disaccharide units, leading to distinct chondroitin sulfate (CS) subtypes.[28,29] Decades of research on nervous system development have elucidated a critical involvement of CSPGs in cell proliferation and differentiation, neural migration, axonal outgrowth, and synapse formation. However, the evidence on how they are involved is complex and at times contradictory, alluding to their structural heterogeneity which enables this wide range of function.[30] As isolated CS polysaccharide components, the immobilization of highly sulfated CS subtypes (CS-D and CS-E) showed higher neurite outgrowth *in vitro via* selective binding to neuronal cell surface integrin receptor αVβ3.[31–33] In addition to this specific bioactivity, the presence of side groups such as the negatively charged sulfate group and the abundance of hydroxyl groups can impart hydrophilicity to the surface after modification. Increased hydrophilicity of a typical hydrophobic electrode surface can prevent non-specific adsorption of plasma proteins, potentially reducing the acute tissue response. This anti-fouling property combined with the specific bioactivity towards neurite outgrowth highlights the suitability of chondroitin sulfate as a bioactive coating for neural microelectrodes.

In this work, we investigated the efficacy of chondroitin sulfate, a novel bioactive coating for neural recording microelectrodes. We hypothesized that the hydrophilic and bioactive coating would prevent non-specific protein fouling while promoting neurite outgrowth. Through these mechanisms, we expect reduced acute inflammation and thus improved chronic recording function for implantable microelectrodes. To test this hypothesis, we performed *in vitro* studies to assess the coating's anti-fouling properties and its specific interactions with primary neuronal and microglial cell cultures. To examine the coating's impact on acute inflammation, we quantified endpoint histology markers after 1-week of *in vivo* implantation. Lastly, we implanted CS-coated and uncoated silicon microelectrodes in the mouse striatum for a week to investigate striatal electrophysiology. We measured impedance and electrophysiological activity on day 1 and day 7 of the implantation to assess the coating's effect on the acute recording performance.

## 2. Materials and methods

### 2.1 Chemicals and reagents

Chondroitin sulfate (CS) from bovine trachea and divinyl sulfone (DVS) were both purchased from Millipore Sigma (Burlington, MA). Ultrapure di-ionized water was used for all experiments (18.2 MΩ, Milli-Q). Glass coverslips (8- and 12-mm diameter) were purchased from Electron Microscopy Sciences (Hatfield, PA). Silicon wafers were ordered from University Wafer (Boston, MA). Non-functional A-style electrodes were purchased from

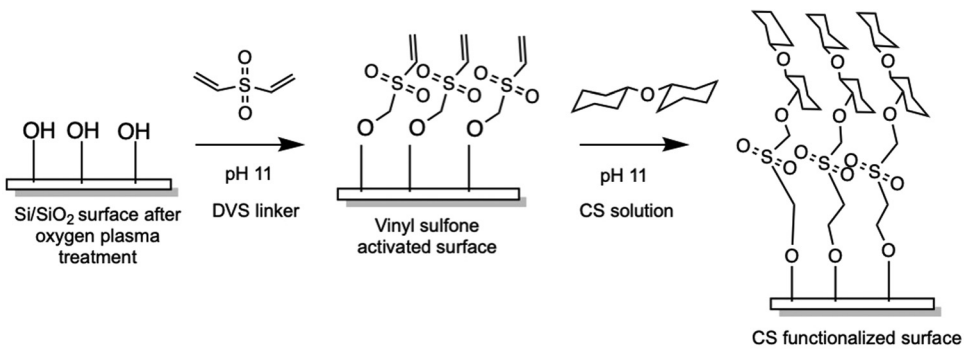


Scheme 1 Immobilization of chondroitin sulfate (CS) on silicon substrates. Smooth silicon substrates treated with oxygen plasma are submerged in divinyl sulfone linker solution, washed, and submerged in CS solution.

 

NeuroNexus (Ann Arbor, MI). The remaining chemical reagents and solvents were purchased from Sigma Aldrich (St. Louis, MO) and used as received without further purification.

### 2.2 Surface immobilization

Chondroitin sulfate was immobilized onto silicon substrates according to the illustration in Scheme 1 *via* the divinyl sulfone (DVS) linker methodology previously described.[34] Before functionalization, glass coverslips were cleaned by sonicating in acetone followed by isopropyl alcohol (IPA), for 10 minutes in each solvent. Silicon wafer substrates were cleaned by submerging in piranha solution (3: 1 $H_2SO_4$: 30% $H_2O_2$) for at least 30 minutes to remove any surface contamination. Cleaned wafers were washed with DI water, and acetone followed by IPA and dried under $N_2$ flow. Cleaned substrates were then activated using $O_2$ plasma for 5 minutes after which they were submerged in 10% DVS solution (v/v, 0.5M carbonate buffer pH 11) for 1 hour at ambient temperature. The DVS-modified surfaces were then thoroughly washed with ~10 mL of water after which they were immersed in chondroitin sulfate solution (100 mg $mL^{-1}$, pH 11 carbonate buffer) at ambient temperature for 16–20 hours. Modified surfaces were then rinsed with ~10 mL water and stored dried until ready for use.

### 2.3 Surface characterization

**2.3.1 X-ray photoelectron spectroscopy (XPS).** XPS measurements were conducted using the ESCALAB 250Xi XPS spectrometer microprobe (Thermo Fisher Scientific, Waltham, MA) with an Al Kα X-ray source (1486.71 eV of photons). The pressure in the analysis chamber was maintained at about $8 \times 10^{-7}$ Pa during each measurement. The survey spectra (from 0 to 1400 eV) and the core-level spectra with higher resolution were both collected. An ion gun was used to compensate for surface charge effects. Three spots on at least two duplicates of samples were analyzed. The software Thermo scientific™ Avantage Data system was used to fit the XPS spectra peaks.

**2.3.2 *In vitro* surface coating stability assessment.** To characterize the coating, its thickness and wettability were investigated. The coating thickness was measured using an ellipsometer (Jobin Yvon Unisel) and the data was fitted with a Cauchy Model using a biofilm refractive index of 1.33.[35] Water contact angles were measured using the Theta Lite optical tensiometer (Biolin Scientific).

After initial measurements, all samples (3–4 silicon wafers per group and time-point) were immersed in phosphate-buffered saline (PBS) for 1, 2, and 4 weeks. Ellipsometry and water contact angle measurements were taken at the end of 1, 2, and 4 weeks after the samples were rinsed with DI water and air-dried. For thickness measurements, there were 22 data points ($n$) for freshly coated CS, $n$ = 29 for a 1-week soak, $n$ = 28 for a 2-week soak, and $n$ = 19 for 4-week-soaked groups. For the water contact angle measurements, there were $n$ = 15 data points for uncoated control, $n$ = 15 for freshly coated CS, $n$ = 15 for a 1-week soak, $n$ = 11 for a 2-week soak, and $n$ = 16 for a 4-week soak. Bare uncoated silicon wafers were used as a control group.

**2.3.3 *In vitro* anti-fouling performance assessment.** Freshly coated CS-substrates and those that had been soaked in PBS for 1, 2, and 4 weeks were then submerged in 2 mg $mL^{-1}$ FITC-albumin solution for 1 hour at room temperature under dark conditions. Samples were then washed with 20 mL of DI water to remove weakly attached proteins and then air-dried. Fluorescence images were captured using a Leica DMI4000 Microscope (Buffalo Grove, IL) with a 3-second exposure time at 10× magnification. A total of 10–15 images were taken across two to three samples that were prepared per condition. The total fluorescence intensities per unit area of the substrates were measured using CellProfiler software (Cambridge, MA).

### 2.4 *In vitro* bioactivity testing

**2.4.1 Neuron cell culture.** Primary neurons from E18 rat fetuses were used to assess the neurite growth-promoting properties of the immobilized CS coating, following the protocols described previously in Woeppel *et al.*[36] Animal experiments were approved by and kept per the University of Pittsburgh Institutional Animal Care and Use Committee standards. Briefly, E18 pregnant Sprague-Dawley rats were euthanized under $CO_2$ followed by cervical dislocation. Rat pups were individually isolated, decapitated, and the cortices were collected. Isolated tissue was then submerged in 0.25% trypsin/EDTA solution for 15 min at 37 °C. The tissue was then washed three times with Hank's balanced salt solution and dissociated *via* trituration. Dissociated suspension was spun at 800 rpm for 10 min at 4 °C and pelleted cells were resuspended in freshly prepared Neurobasal media supplemented with B27, GlutaMAX, penicillin–Streptomycin (Gibco) and counted. Cells were plated at a density of 30 000 cells $cm^{-2}$ on 12-mm diameter glass coverslips coated with 100 mg $mL^{-1}$ CS and grown for 48 hours before they were fixed with 4% paraformaldehyde (PFA). Fixed cells were permeabilized with 0.1% Triton-X in PBS, followed by immunostaining for beta-III-tubulin and nuclei. Images were taken with Leica DMI 4000B fluorescence microscope at 20× magnification. 3–4 images were taken per well, with three wells per condition and the cell culture experiment was repeated four times. Neurite outgrowth was quantified using the Neurite Tracer plug-in on ImageJ.[37]

**2.4.2 Microglia cell culture.** Primary microglia cells from neonatal rat cortices were used to investigate the effect of the CS-coating on microglia *in vitro*. Animal experiments were approved by and kept per the University of Pittsburgh Institutional Animal Care and Use Committee standards. 1–2-day-old neonatal pups were anesthetized by burying them in ice for 5–10 minutes. The pups were decapitated, and the brains were carefully excised. Isolated cortices were transferred to a 15 mL tube containing ice-cold HBSS, and triturated until the suspension was homogenous. The solution was then filtered through a 70 μm cell strainer and centrifuged for 10 minutes at 1200 rpm. The pelleted cells were resuspended in Dulbecco's Modified Eagle medium/nutrient mixture F12 media (Gibco) and the resulting mixed glia cells were plated in T-175 flasks and grown until confluency (12–14 days). Microglia were collected by shaking the mixed glia-containing flask for 1 hour at 180 rpm

in a MaxQ8000 HP (ThermoFisher, Waltham, MA). The collected media was then centrifuged again at 950 rpm, 25 °C for 10 minutes. Pelleted microglia were resuspended in complete DMEM media and plated at a density of 30 000 cells $cm^{-2}$ on glass coverslips coated with 100 mg $mL^{-1}$ chondroitin sulfate solution for 24 hours before performing other *in vitro* assays. Uncoated glass coverslips were used as control.

**2.4.3 Cell staining and imaging.** Microglia cells cultured on CS-coated and uncoated glass coverslips were fixed with 4% paraformaldehyde (PFA) and permeabilized with 0.2% Triton-X, followed by immunostaining with Iba-1 and DAPI. Using the Leica DMI 4000B microscope, 3 images per well were taken for three wells per condition at 20× magnification. CellProfiler was used for the quantification of Iba-1 positive cells.

**2.4.4 Microglial phagocytosis assay.** Microglia phagocytosis assay was performed according to the published protocol by Lian *et al.*[38] Briefly, 1 μm fluorescently labeled latex beads (Sigma) were pre-opsonized in fetal bovine serum for 1 hour at 37 °C and diluted with complete DMEM media (0.1% v/v). Microglia media was replaced with the bead-containing media and the cells were incubated at 37 °C for 1–2 hours. Cells were thoroughly washed with ice-cold PBS five times, fixed with 4% PFA, and stained for Iba-1 and DAPI. Three images were taken per well with three wells per condition. Cells expressing Iba-1, DAPI, and the beads were manually counted as phagocytosis-positive cells. To get the % phagocytic cells, the number of phagocytic cells was divided by the total number of microglia.

### 2.5 *In vivo* bioactivity testing

**2.5.1 Animal surgeries.** For the acute *in vivo* histology study, five C57BL/6 male mice (Jackson Laboratory, Bar Harbor, ME) were bilaterally implanted with non-functional A-style silicon probes (3 mm length, NeuroNexus, Ann Arbor, MI) with a total of 5 control (uncoated) and 5 CS-coated arrays for 1-week. For the electrophysiological study, eight female mice were implanted with NeuroNexus (A1x16-5 mm-100-703-CM16) electrodes, where four mice were implanted with an uncoated control probe, and four mice were implanted with a CS-coated electrode for a week. For this cohort, mice were housed on a 12/12 light/dark cycle (lights on 7 a.m., lights off 7 p.m.) with food and water *ad libitum*. *ClockΔ19* mice on a Balb/c mixed background were bred as heterozygotes to produce wild-type and homozygous mutant littermates. Only the female, wild-type mice 15–19 weeks old from these litters were used for the study. The mutant mice were used for a separate ongoing study. Throughout the study, animal experiments and housing were approved by and kept in accordance with the University of Pittsburgh Institutional Animal Care and Use Committee standards.

For both the acute histology and the electrophysiology studies, the same procedures were used, except for the type of implanted electrode device (functional vs non-functional) and implantation coordinates. Animals were anesthetized using an isoflurane vaporizer (2% in oxygen for induction, 1.5% for the remainder of the surgery) and the state of anesthesia was closely monitored by observing the respiratory rate and the absence of pedal reflex. After induction, the animal was mounted to a stereotactic frame (Kopf Instruments, Tujunga, CA) and placed on top of a heating pad (TP1500, Adroit Medical Systems, Loudon, TNP) at 37 °C. The head was shaved and sterilized with iodine and ethanol three times and an ophthalmic ointment was applied to the eyes. After placing a sterile drape over the surgical area, an incision was made to expose the bregma and lambda sutures of the skull. For the acute study, in reference to the coronal suture, electrode implantation holes were made bilaterally 4 mm posterior to bregma, 3 mm distal from the midline using a surgical drill (0.7 mm tip diameter drill bit, Fine Science Tools, Inc., Foster City, CA). Sterile saline washes were applied continuously to dissipate the heat produced by drilling. Two bone screws (stainless steel; shaft diameter 0.96 mm, length 2 mm, Bioanalytical Systems Inc., West Lafayette, IN) were screwed into the newly created holes with careful attention not to pierce through to the brain. Two electrode holes were drilled with the same drill bit, the coated and non-coated non-functional probes were bilaterally inserted using Neural Glider (Actuated Medical, Bellefonte, PA) at a rate of 0.05 mm $s^{-1}$ to a depth of 1.5 mm.

For the electrophysiology study, three bone screws (stainless steel; shaft diameter 0.96 mm, length 2 mm, Bioanalytical Systems Inc., West Lafayette, IN) were utilized to ground the functional electrode device as well as to stabilize the dental cement head cap. In reference to bregma, the implantation site was 1.5 mm anterior, and 1 mm distal. Insertion was supported by Neural Glider at a rate of 0.05 mm $s^{-1}$ to a depth of 4.5 mm. Once inserted, the probe holes were sealed using Kwik-Cast Sealant (World Precision Instruments, Sarasota, FL). UV-curable dental cement (Pentrol Clinical, Orange, CA) was generously applied. Topical antibiotic was applied around the incision sites and an intraperitoneal injection (i.p.) of 5 mg $kg^{-1}$ Ketofen (100 mg $ml^{-1}$, Zoetis Inc, Kalamazoo, MI) was delivered. Mice were placed on a heating pad and allowed to recover. Ketofen injections (5 mg $kg^{-1}$) were administered daily for three days after the surgery.

After 1 week of implantation, animals were administered an i.p. overdose of ketamine/xylazine (80–100 mg $kg^{-1}$ and 5–10 mg $kg^{-1}$, respectively) and transcardially perfused with 4% (v/v) PFA in PBS once they were unresponsive to toe pinches. Mice were decapitated and the skulls were removed to post-fix the brain in 4% PFA at 4 °C for 4–6 hours. The skulls with the probes still attached were preserved for explant analysis. Brains were then soaked in a 15% sucrose solution for 24 hours followed by submerging in a 30% sucrose solution until the brains sunk to the bottom of the tube (usually 24–48 hours). Brains were then carefully frozen in a 2 : 1 ratio, *i.e.*, 20% sucrose in PBS : optimal cutting temperature compound (Fisher HealthCare, Houston TX). Frozen tissue sections were horizontally sectioned into 25 μm thick sections normal to the tract of the probes using a cryostat (Leica CM1950, Buffalo Grove, IL).

**2.5.2 Electrophysiological measurements and analysis.** Impedance measurements were taken with a Potentiostat (Metrohm PGSAT128N) before the coating modification and after implantation on a weekly schedule. In addition, weekly spontaneous neural recordings (5 minutes) were taken with an

 

RX7 acquisition system (Tucker Davis Technologies, Alachua, FL) and a Medusa Pre-amplifier (Tucker Davis Technologies). Impedance measurements lower than 20 kΩ and higher than 2000 kΩ were excluded. Animals were administered 2% isoflurane for induction, after which isoflurane was reduced to 1% to maintain a lightly anesthetized state.

Neural data analysis was based on previously published work.[39] The raw neural recording data was filtered between 300–10 000 Hz and threshold crossing events were identified by applying a negative threshold value of 3.5 standard deviations. To identify single units, Plexon offline sorter (Plexon Inc, Dallas TX) was used and the *k*-means clustering method was applied (with an adaptive standard EM 2 to 5). Using a 3D PCA feature space, individual single units were manually inspected. Noise was defined as the standard deviation of the raw data stream, with the spikes included since the spike rate was found to be minimal. The signal-to-noise ratio (SNR) was then calculated as the ratio between the peak-to-peak amplitude (p2p) of the sorted single units divided by noise. We assigned an SNR of 0 to channels with no sortable units. The overall SNR was calculated as the average of all channels, while the active SNR averaged only non-zero SNR values across all channels. The single unit (SU) yield was calculated as the number of electrode sites recording at least one sorted unit divided by the total number of channels (16), multiplied by 100 to obtain a percentage. Custom MATLAB scripts were used to calculate the p2p, SNR, and SU yield and GraphPad Prism was used for performing statistical analysis and for plotting the results.

**2.5.3 Histology.** Tissue sections were rehydrated in citrate buffer, blocked with 10% goat serum, and then treated with 0.1% Triton-X for 45 minutes. Tissue sections were stained across a depth of 1900 microns for NeuN (Millipore mouse 1:250), Iba-1 (Millipore mouse 1:500), GFAP (DAKO rabbit 1:500), and blood–brain barrier injury marker for immunoglobulin G (IgG) (Alexa Fluor 647-conjugated AffiniPure Fab Fragment). The chosen stains were intended to detect the presence of activated microglia (Iba-1), reactive astrocytes (GFAP), neuronal density (NeuN), and blood–brain barrier injury (IgG). Comparisons were made between the uncoated control and CS-coated probe groups based on the relative intensities of these markers around the implanted probes.

**2.5.4 Histological analysis.** Imaging was performed on a confocal microscope (Olympus Fluoview 3000, Olympus Life Science, Waltham, MA) to evaluate differences in immune markers surrounding the implant sites. Image analysis was performed using a custom MATLAB script as published by Kozai *et al.*[40] Briefly, bins of 10 microns were created concentrically around the probe implant, and the intensity of the stain or the number of cells per bin (counted manually for NeuN) were measured. Since NeuN were manually counted, the neuronal density was represented as averages across 50-micron bins to avoid cell counting ambiguity near the probe. Intensities and counts were scaled to the corners of the images. The background intensities were also calculated from the corners of the image (20% of the total image area) by removing pixels greater than 1 standard deviation (STD) above the mean and then calculating the mean and variance of the remaining pixels. All pixels that were greater than 1 STD above the mean background intensity were used for the analysis.

### 2.6 Explant analysis

Explant analysis was performed to examine and compare the extent of tissue coverage on the explanted probes with and without the CS coating. The explanted probes were carefully detached from the skull and submerged in 100% ethanol for 5 days, followed by air-drying for 2 days. Probes were then pressed flat on conductive tape and sputter coated with 5–10 nm of gold–palladium coating in preparation for taking images on the scanning electron microscope (SEM). For quantification of biological tissue coverage on the explanted probes, grids were inserted on the SEM image using ImageJ grid function. The number of grids with visible tissue coverage was divided by the total number of grids covering the electrode pixel area and reported as % tissue coverage area for both control ($n$ = 4 images) and CS groups ($n$ = 5 images). Welch's $T$-test was performed for statistical comparison.

### 2.7 Statistics

For all statistical tests, GraphPad Prism 10.0 was used. For *in vitro* and *in vivo* studies, unless otherwise stated, one-way ANOVA and two-way ANOVA (wherever appropriate) with Tukey's *post hoc* analysis were used. For the recording analysis, a mixed model for repeated measures (MMRM) was used. Data was described as the mean ± standard error of the mean unless stated otherwise.

## 3. Results

### 3.1 Immobilization of CS and characterization

Chondroitin sulfate (CS) was immobilized onto silicon or silicon dioxide surfaces *via* divinyl sulfone (DVS) linker chemistry (Scheme 1), where DVS serves as a linchpin between hydroxyl-terminated silicon surfaces and the hydroxyl-bearing polysaccharide. Before the functionalization, silicon (Si) wafer substrates were treated with piranha solution, followed by acetone and isopropanol to remove larger contaminants. Si substrates were treated with $O_2$ plasma treatment to activate the surface by introducing hydroxyl groups, followed by the addition of the DVS linker and finally the CS solution. Immobilization of CS was monitored stepwise *via* X-ray photoelectron Spectroscopy (XPS), ellipsometry (Fig. 1), and water contact angle (WCA) (Fig. 2), to measure changes in the chemical bonding, thickness of the immobilized coating, and hydrophilicity, respectively.

High-resolution XPS characterization (Fig. 1(A)–(E)) showed Si 2p, C 1s, and O 1s peaks for the uncoated bare control at 106.59, 287.55, and 534.52 eV respectively, and their atomic % were 27.57%, 13.78%, and 58.65%. For the DVS condition, the peaks for Si 2p, C 1s, O 1s, and S 2p were 106.34, 286.70, 533.84, and 172.23 eV, and their subsequent atomic % were 8.75%, 7.36%, 31.46%, 0.23%. Finally, after the CS immobilization, the

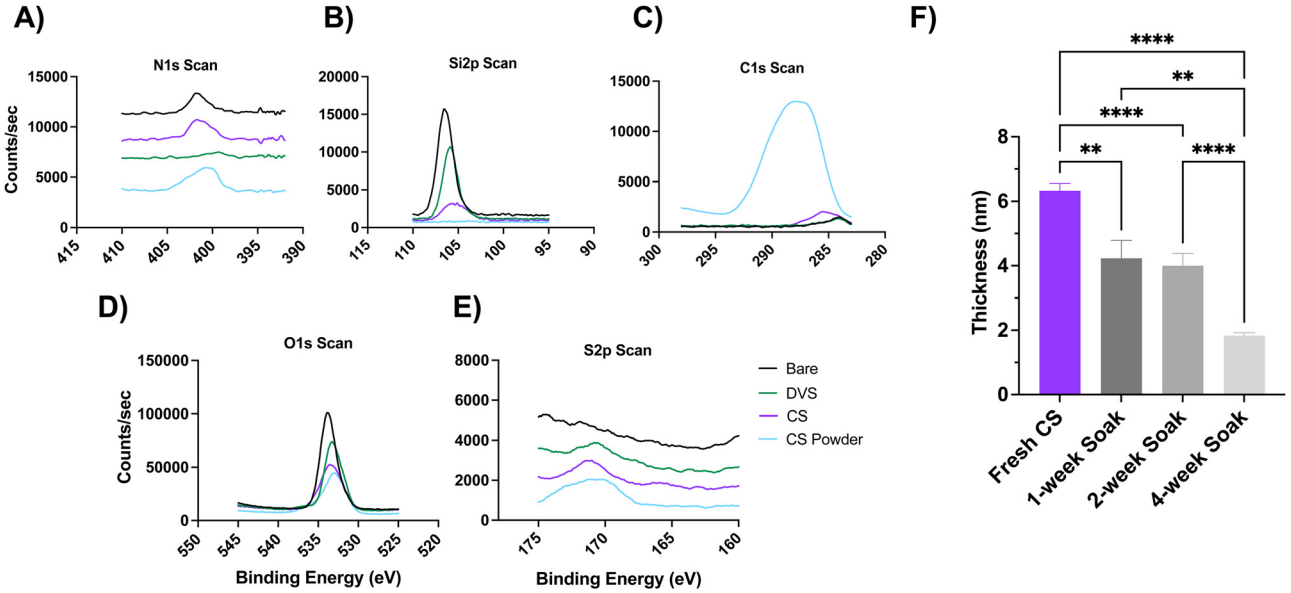


Fig. 1 Surface characterization of CS-coated substrates. (A)–(E) High-resolution scans of N1s (A), Si2p (B), C1s (C), O1s (D), and S2p (E) using X-ray photoelectron spectroscopy (XPS). (E) Measurement of coating thickness (nm) of freshly CS-modified silicon wafer and CS-coated samples soaked in PBS at room temperature for 1, 2, and 4 weeks. One-way ANOVA $^{**}p < 0.01$, $^{****}p < 0.0001$. Data is mean ± SEM.

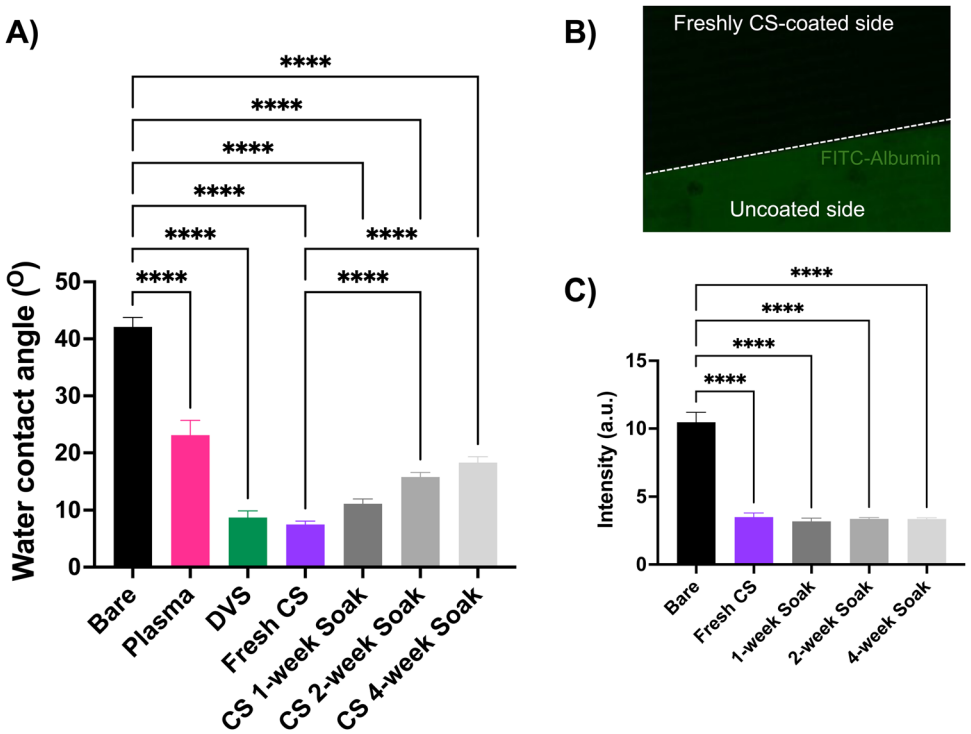


Fig. 2 Assessment of hydrophilic property of immobilized CS coating. (A) Water contact angle (°) measurements for bare silicon wafer, plasma-treated wafer, DVS-linker modified wafer, freshly CS-coated wafers, and CS-coated wafers soaked for 1, 2 and 4 weeks in saline. (B) Representative image showing the distinction in the protein fouling, shown by pseudo-colored FITC-albumin for freshly coated CS side and the uncoated side on the same piece of silicon wafer. (C) Quantified fluorescence intensity (a.u.) from unmodified bare silicon wafer serving as control, freshly coated CS silicon wafers and CS-coated samples soaked in PBS at room temperature for 1, 2 and 4 weeks. One-way ANOVA with Tukey's multiple comparison test, $^{****}p < 0.0001$ for both (A) and (C). Data is mean ± SEM.

atomic peaks for Si 2p, C 1s, O 1s, S 2p, and N 1s were 105.72, 287.64, 534.10,171.81, 401.91 eV and the atomic % were 2.44%, 23.25%, 21.29%, 0.56%, and 1.28%. Additionally, we used chondroitin sulfate powder as a positive control, and the C

 

1s, O 1s, S 2p, and N 1s peaks were 287.99, 533.88, 170.99, 401.31 eV with their atomic % as 51.57%, 41.20%, 1.90%, and 5.32%, respectively. The calculated ratio between nitrogen and sulfur based on the experimental atomic % was 0.36 for the CS powder and 0.44 for the immobilized CS (theoretical ratio of N:S is 0.44). Overall, the successful immobilization of CS is indicated by the presence of additional S 2p and N 1s peaks in the CS condition as compared to the uncoated bare control, the decrease in the atomic % for Si 2p in the CS condition, and the comparison to the CS powder control.

To assess the stability of the immobilized CS, coated samples were soaked in phosphate buffer saline (PBS) solution at room temperature for 1, 2, and 4 weeks, and the changes in coating thickness and hydrophilicity were measured (Fig. 1(F) and 2). Freshly coated substrates had a starting thickness of around 6.3 ± 0.22 nm (mean ± standard error of mean), which significantly decreased to 4.2 ± 0.56, 4 ± 0.38, 1.8 ± 0.089 nm for samples soaked for 1, 2, and 4 weeks, respectively ($p < 0.01$, $p < 0.0001$, and $p < 0.0001$ one-way ANOVA, respectively) (Fig. 1(F)). Despite the gradual degradation due to soaking, the remaining coating is still within the expected 2–3 nm range of similar polysaccharide-based coatings reported in literature.[35,41]

The water contact angle (WCA) measurements describe the hydrophilicity of the modified substrates. As compared to the uncoated bare control, after the oxygen plasma treatment, the WCA dramatically decreased from 43.5° ± 5.1 to 23.1° ± 4.5 (mean ± standard deviation (SD)). The WCA subsequently dropped after the DVS reaction (8.7° ± 2) and was observed to be the lowest after the CS immobilization (6.5° ± 1.6) as compared to the uncoated Si wafer ($p < 0.0001$, one-way ANOVA) (Fig. 2(A)). This suggests the addition of the CS coating imparts a hydrophilic property to the otherwise hydrophobic Si/$SiO_2$ surface. As compared to the freshly coated CS substrates, there was no significant increase in the WCA for samples soaked for one week, however, a significant change in WCA was observed when soaked for 2 and 4 weeks at room temperature. This increase in WCA represents the slight decrease in the hydrophilicity of the substrate, as some portion of the coating starts to degrade in solution. However, the coating remains significantly more hydrophilic as compared to the uncoated Si wafer, suggesting the stability of the coating in the tested soaking conditions.

Neural tissue interfacing devices coated with a hydrophilic layer can help reduce the non-specific adsorption of the blood proteins on the implant surface, a key first step in the foreign body response.[3,42] We performed a protein adsorption test by soaking the uncoated Si wafer, freshly CS-coated, and soaked (1, 2, and 4-week) substrates in fluorescently tagged albumin protein and quantified the intensity of the adsorbed protein on these substrates (Fig. 2(B) and (C)). A significant decrease in the intensity (arbitrary units, a.u.) of the adsorbed protein for the freshly coated wafers (3.5 ± 0.9 a.u.) indicated a drastic anti-fouling effect of the coating as compared to the uncoated control (10.5 ± 2.8 a.u.) ($p < 0.0001$, one-way ANOVA). This anti-fouling effect of the coating persisted even after the CS-coated substrates were soaked for 1 (3.18 ± 0.6 a.u.), 2 (3.36 ± 0.3 a.u.), and 4 weeks (3.35 ± 0.2 a.u.) and no significant increase in FITC-albumin was found in the soaked samples, when compared to the freshly coated samples (Fig. 2(B)).

### 3.2 Investigating coating's bioactive effect *in vitro*

**3.2.1 Improvement in neurite attachment and outgrowth.** To examine the bioactive effect of the CS-coating, we cultured primary neurons on the CS-coated substrates and compared the neurite attachment and outgrowth to the control substrates. Cultured neurons were grown for 48 hours, followed by fixation and staining for β(III)-tubulin (neurons) and 4′,6-diamidino-2-phenylindole (DAPI) (nuclei). While neurites were visible on all substrates, they were particularly longer on the CS-coated substrates (Fig. 3). As compared to the uncoated bare control, CS-coated substrates promoted neurites to be over four times longer ($p < 0.0001$, one-way ANOVA with Tukey's *post hoc*). Moreover, the neurite outgrowth on CS-coated substrates was significantly higher than that observed on the laminin-coated substrates (positive control), a glycoprotein known to support growth and differentiation of neural cells ($p < 0.05$, one-way ANOVA with Tukey's *post hoc*).

**3.2.2 Reduction in microglia attachment and activity.** Primary microglia were cultured on uncoated and CS-coated substrates and the viability of cultured cells was assessed using calcein (live cells) and propidium iodide (dead cells) dyes (Fig. 4(A)–(C)). Overall, the cell viability of cultured microglia was significantly lower on CS-coated substrates as compared to the uncoated control ($p < 0.0001$, two-way ANOVA with Tukey's *post hoc*). There was no significant difference between the live and dead cell count $mm^{-2}$ for microglia growing on CS-coated

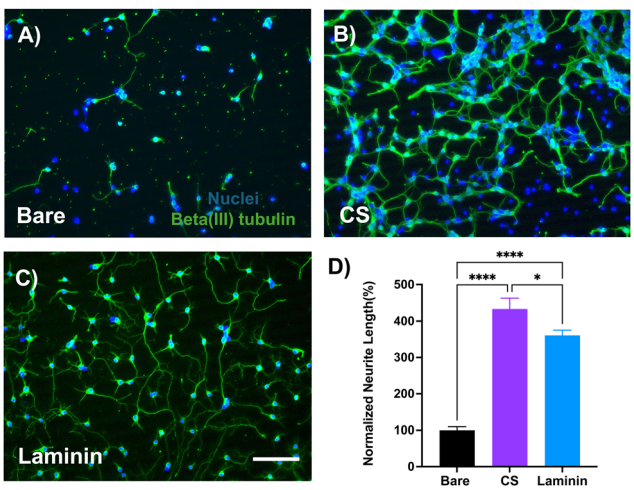


Fig. 3 CS-coated substrates promote neurite attachment and outgrowth. Representative images of neurites (beta-III tubulin) growing on (A) Bare uncoated glass coverslips (B) CS-modified glass coverslip (C) and laminin-treated well plate (positive control). (D) Quantification of beta(III) tubulin expressing neurites, normalized neurite length (%) to bare uncoated glass coverslips. One-way ANOVA with Tukey's multiple comparisons test, *$p < 0.05$, ***$p < 0.0001$. Four independent cell cultures were performed with three technical replicates in each round, with total $n = 41$ images for Bare group, $n = 48$ images for CS group, and $n = 45$ for laminin group were analyzed. Scale bar is 100 microns. Data is mean ± SEM.

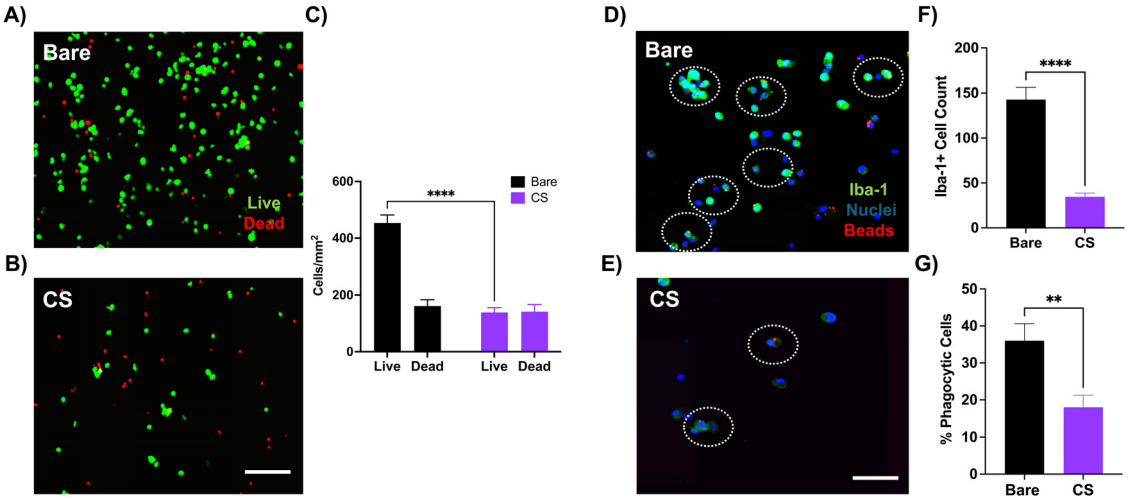


Fig. 4 Effects of CS-coated substrates on microglial viability and phagocytosis. Representative images of primary microglia growing on (A) bare uncoated glass coverslips and (B) CS-coated glass coverslips. The live cells were stained by calcein (green), and dead cells were stained by propidium iodide dye (red). (C) Quantification of live and dead cells growing on each type of surface. Two-way ANOVA with Tukey's multiple comparison test, $^{****}p < 0.0001$. Representative images of phagocytosis assay performed on primary microglia growing on (D) bare uncoated coverslips and (E) CS-coated glass coverslips with Iba-1+ cells shown in green, nuclei by DAPI, and latex beads by red. White circles highlight the Iba-1+ cells which phagocytosed the fluorescent latex beads. (F) Quantification of the absolute number of Iba-1+ cells. (G) Quantification of the % of cells that performed phagocytosis for all the Iba-1+ cells counted in the samples. Welch's *T*-test, $^{****}p < 0.0001$, $^{**}p < 0.01$. Three independent cell cultures were performed with three technical replicates in each round, with total $n = 27$ images analyzed for both Bare and CS conditions. Scale bar is 100 microns. Data is mean ± SEM.

substrates. We also performed a phagocytosis assay to determine the coating's effect on the cultured microglia to perform phagocytosis. We counted the number of Iba-1+ cells that ingested fluorescently labeled latex beads and calculated the percentage of microglia cells that performed phagocytosis for the entire population of the Iba-1+ cells (Fig. 4(D) and (E)). Significantly fewer microglial cells were growing on CS substrates (Fig. 4(F)) ($p < 0.0001$, Welch's *T*-test), and of those, significantly fewer microglia performed phagocytosis as compared to those growing on the uncoated control substrates (Fig. 4(G)) ($p < 0.01$, Welch's *T*-test).

### 3.3 Investigating coating's bioactive effect *in vivo*

**3.3.1 Increased neuronal density and neurofilament around CS-coated implant.** To investigate the effect of the coating on the neuronal population and acute inflammation *in vivo*, we bilaterally implanted coated and uncoated non-functional silicon planar arrays in C57BL/6J mouse cortex for 1-week. We then performed immunohistochemistry to assess the density of neuronal population (NeuN) and axonal neurofilament (NF200) around the coated and uncoated implant sites (Fig. 5). A significantly elevated population of neurons was observed up to 150 microns of the coated implant site as compared to the uncoated implant ($p < 0.0001$, two-way ANOVA, Sidak's multiple comparison test). Similarly, a significant increase in the neurofilament expression for up to 150 microns away from the coated implant was observed ($p < 0.0001$, two-way ANOVA, Sidak's multiple comparison test). These *in vivo* observations follow the trend of increased neurite attachment and growth demonstrated in the *in vitro* experiments.

**3.3.2 Reduced inflammatory response around CS-coated implant.** We examined the extent of microglial activation (Iba-1), astrocytic reactivity (GFAP), and blood–brain barrier (BBB) leakage (IgG) by quantifying the fluorescence intensity of these markers as a function of distance from the implant (Fig. 6). We observed significantly lower microglial activation around the coated implant as compared to the uncoated control for up to 40 microns away from the probe hole ($p < 0.0001$, two-way ANOVA, Sidak's multiple comparisons test). Beyond 50 microns, the microglial intensity returned to the baseline intensity for both groups, illustrating the localized activation around the probe.

We observed increased co-localization of microglia (Iba-1) and neurons (NeuN) close to the probe hole in the control group as compared to the CS group (ESI,† Fig. S2). While qualitative, this observation could suggest increased engulfment of stressed neurons by activated microglia, a phenomenon previously reported.[43,44]

The GFAP encapsulation was similar for both coated and uncoated probes. Though not significant, the GFAP intensity was lower around coated implants 90–140 microns away from the implant site as compared to the control. The observed trend of increasing reactivity as the distance from the site increases could be attributed to the early time-point of 1 week, at which the astrocytes are starting to migrate towards the injury but the tissue around the implant site is mostly occupied with activated microglia.

The IgG protein staining was overall significantly lower around the coated probes up to 130 microns away from the implant site as compared to the control probe ($p < 0.0001$, two-way ANOVA). This difference was the most drastic up to 40 microns away from the implant, after which the intensity started to return to baseline. This observation illustrates the hydrophilic effect of the coating which is likely reducing the non-specific protein adsorption of the IgG protein upon the blood–brain barrier rupture during insertion.

 

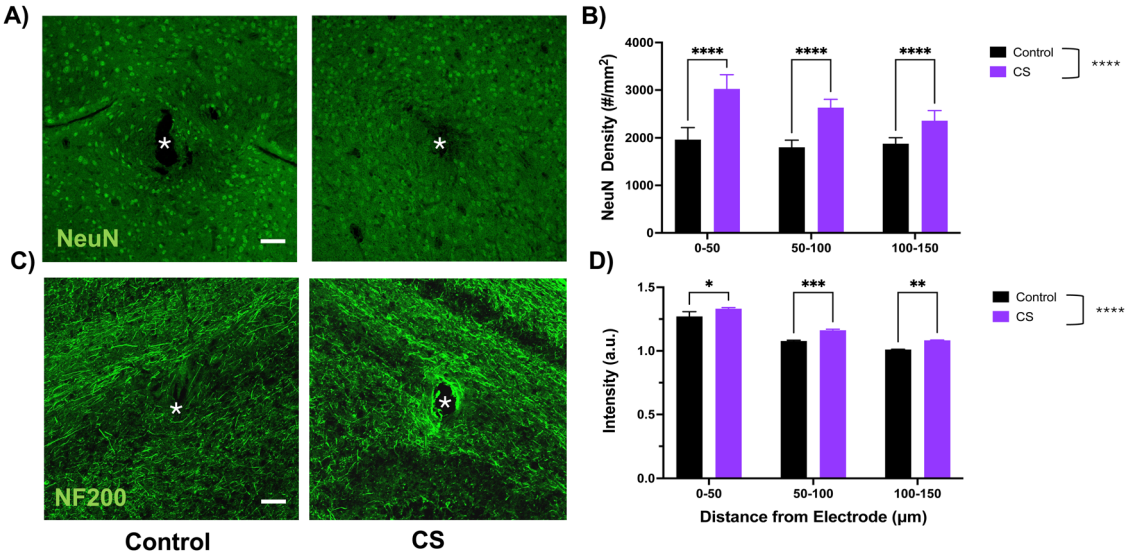


Fig. 5 Increased neuronal population and neurofilament expression around CS-coated electrodes. (A) Representative images showing neuronal nuclei (NeuN) density around the implant site (shown by *) for control (left) and CS-coated (right) electrodes. (B) Quantification of the neuronal density (number of NeuN+ cells per $mm^2$) as a function of distance from the electrode (μm) in three bin-categories, 0–50 μm, 50–100 μm, 100–150 μm. Two-way ANOVA with Sidak's multiple comparison test, $****p < 0.0001$. $n$ = 12 images for control group, $n$ = 10 images for CS group. (C) Representative images showing neurofilament (NF200) expression around the implant site (*) for the control (left) and CS group (right). (D) Quantification of NF200 intensity expression as a function of distance from the electrode (μm) in three bin-categories, 0–50 μm, 50–100 μm, 100–150 μm. Two-way ANOVA with Sidak's multiple comparison test, $*p < 0.05$, $**p < 0.01$, $***p < 0.001$, $n$ = 14 images analyzed for control group, $n$ = 18 images analyzed for CS-group, $N$ = 5 animals per group. Scale bar is 100 microns. Data is mean ± SEM.

### 3.4 Explant analysis after acute implantation

After the completion of the acute 1-week implantation study, probes were carefully explanted and serially dehydrated in ethanol and prepared for scanning electron microscopy (ESI,† Fig. S1). Images were taken to compare the tissue coverage on explanted control and CS probes. Upon quantification, we found that 86.5 ± 3.34% of the uncoated control probe surface was covered with biological matter as compared to only 37 ± 1.71% in the CS group (Welch's $T$-Test, $****p < 0.0001$, mean ± SEM). This biological matter is likely composed of blood plasma proteins and encapsulation tissue. This reduction in tissue coverage is likely to be the effect of the hydrophilic and anti-fouling CS coating.

### 3.5 Characterization of recording performance *in vivo*

After observing the coating's neurite growth-promoting property *in vitro* and a reduced acute inflammatory response *in vivo*, we proceeded to evaluate whether these observations would translate to improved recording quality. We hypothesized that an increase in the neuronal density around the coated electrode would potentially enhance single unit yield due to higher number of viable neurons near the implant. To test this, we implanted CS-coated and uncoated 16-channel single-shank NeuroNexus electrode arrays in mice and performed impedance and electrophysiological recordings. We compared impedance and recording performance, as collectively defined by the peak-to-peak amplitude, noise floor, signal-to-noise ratio, and single-unit yield (*i.e.*, % of channels recording at least one single unit) over the course of a week.

We first measured the impedance before and after coating the electrodes and found a significant decrease in the impedance (pristine: 363 ± 19 kΩ, post-coating: 288 ± 38 kΩ, $p$ = 0.04, Student's $T$-test, mean ± SEM), likely due to the increased wettability of the electrode site.[45] However, this change in impedance is only a 20% difference and is not expected to affect the electrical function of the implanted probes. The first impedance measurement after implantation was on day 1 which showed a characteristic dramatic increase in impedance for both the control (103% increase) and coated electrodes (37% increase) due to the addition of tissue impedance. The impedance for the CS group for day 1 and day 7 was significantly lower than the control group and no significant difference was found between the CS groups between day 1 and day 7 indicating stable impedance (Fig. 7(C)).

While both groups recorded sortable single units (Fig. 7(A) and (B)), the average peak-to-peak amplitude of the sorted single units was overall significantly higher in the control group (61.26 μV) across both time points as compared to the CS group (45.71 μV) ($p < 0.0001$, two-way ANOVA) (Fig. 7(E)). The noise was overall significantly lower for the CS group as compared to the control ($p < 0.0001$, two-way ANOVA) and significantly lower for the Day 7 time point ($p < 0.0001$, two-way ANOVA). (Fig. 7(D)). The background noise and peak-to-peak amplitude directly contribute to the calculated signal-to-noise (SNR) ratio (Fig. 7(F) and (G)). The overall SNR (Fig. 7(F)) which includes channels with no sortable units (with the SNR set to 0) starts higher on day 1 but declines on day 7, with no overall or time-point-dependent significant difference. Despite having lower single unit (SU) amplitude, the CS group had similar SNR values to the control group due to the significantly lower noise floor levels. The active SNR which only includes the channels

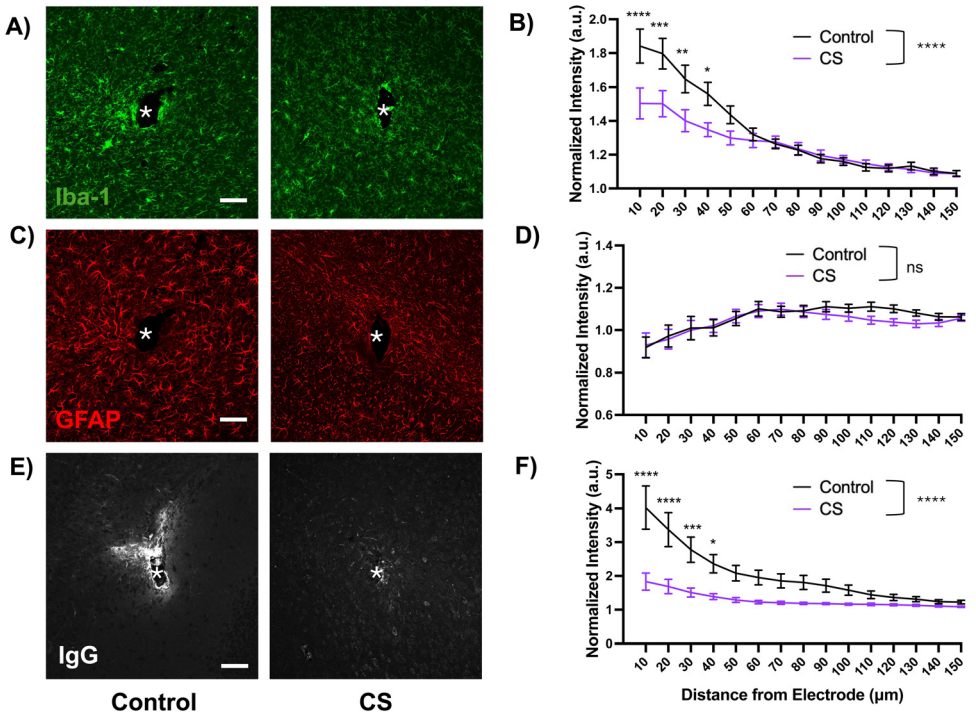


Fig. 6 Reduced acute inflammatory response around CS-coated electrodes. (A) Representative images showing microglia activation (Iba-1) around the control (left) and CS (right) implant site (*). (B) Quantification of the microglial normalized intensity as a function distance from the electrode implant. We found overall significance between groups for all distance bins and significance for groups up to 40 microns away from the implant. $n$ = 39 images analyzed for control; $n$ = 38 images analyzed for CS group. (C) Representative image showing astrocytic reaction around control (left) and CS (right) implant site (*). (D) Quantification of normalized astrocytic reactivity as a function of distance from the implant, $n$ = 27 images for control and $n$ = 24 images were analyzed for CS. (E) Representative images showing IgG fouling near the control (left) and CS (right) implant site (*). (F) Quantification of the normalized IgG intensity as a function of distance from the implant, $n$ = 16 images were analyzed for both control and CS groups. Normalized intensity is in arbitrary units (a.u.). There was an overall significant difference between the groups, as well as a significant difference for up to 40 microns from the implant. Two-way ANOVA with Sidak's multiple comparison tests were used for statistical analysis, *$p < 0.05$, **$p < 0.01$, ***$p < 0.001$, ****$p < 0.0001$, ns = not significant. $N$ = 5 animals per group (control and CS).

recording sortable units (Fig. 7(G)) followed a similar trend for both groups over the two time points. The % channels that record at least one sortable SU produce the SU yield (Fig. 7(H)), which was found to be overall significantly higher in the CS group (74.2%) than the control group (67.2%) and at the day 1 time point but ($p < 0.01$, two-way ANOVA) were not significantly different on day 7.

# 4. Discussion

The host tissue response experienced by implanted electrodes is one of the main factors reducing the effectiveness of the neural interface. While several strategies have been investigated, surface coatings have demonstrated immense potential in modulating this undesired local immune response. Hydrophilic zwitterionic coatings show significantly reduced non-specific protein fouling which helps to reduce the immune response, but do not offer bioactivity towards the native tissue.[9,10] Protein-based bioactive coatings, such as L1, can address this issue and provide several benefits, however, the production process itself can be challenging.[16,18] This work explores the use of a commercially available chondroitin-sulfate-based coating, which not only provides anti-fouling and bioactive benefits but can be functionalized on the device surface through a simple process. We first characterized the immobilized coating *via in vitro* assays, which was followed by evaluating the acute *in vivo* tissue response. Finally, we compared the recording quality of CS-coated electrodes to uncoated controls during a week-long implantation study in the striatum.

## 4.1 Stability of the coating

It is critical to test the stability of a coating that is expected to operate in a complex biological environment. We soaked coated substrates in saline buffer for 1, 2, and 4 weeks at room temperature, and evaluated the changes in coating thickness, hydrophilicity, and anti-fouling properties. As the soak time increased, we did observe a gradual decrease in the coating thickness, and a corresponding decrease in the wettability, as compared to freshly coated surfaces. However, the coating thickness was still in the expected range for covalently linked polysaccharide coatings[35,41] and the water contact angle remained significantly lower than the uncoated controls. Moreover, despite the slight deterioration of the coating after soaking, its anti-fouling effect was sustained for 4 weeks, as no significant difference was found in the amount of non-specifically adsorbed fluorescently labeled protein when compared to freshly coated

 

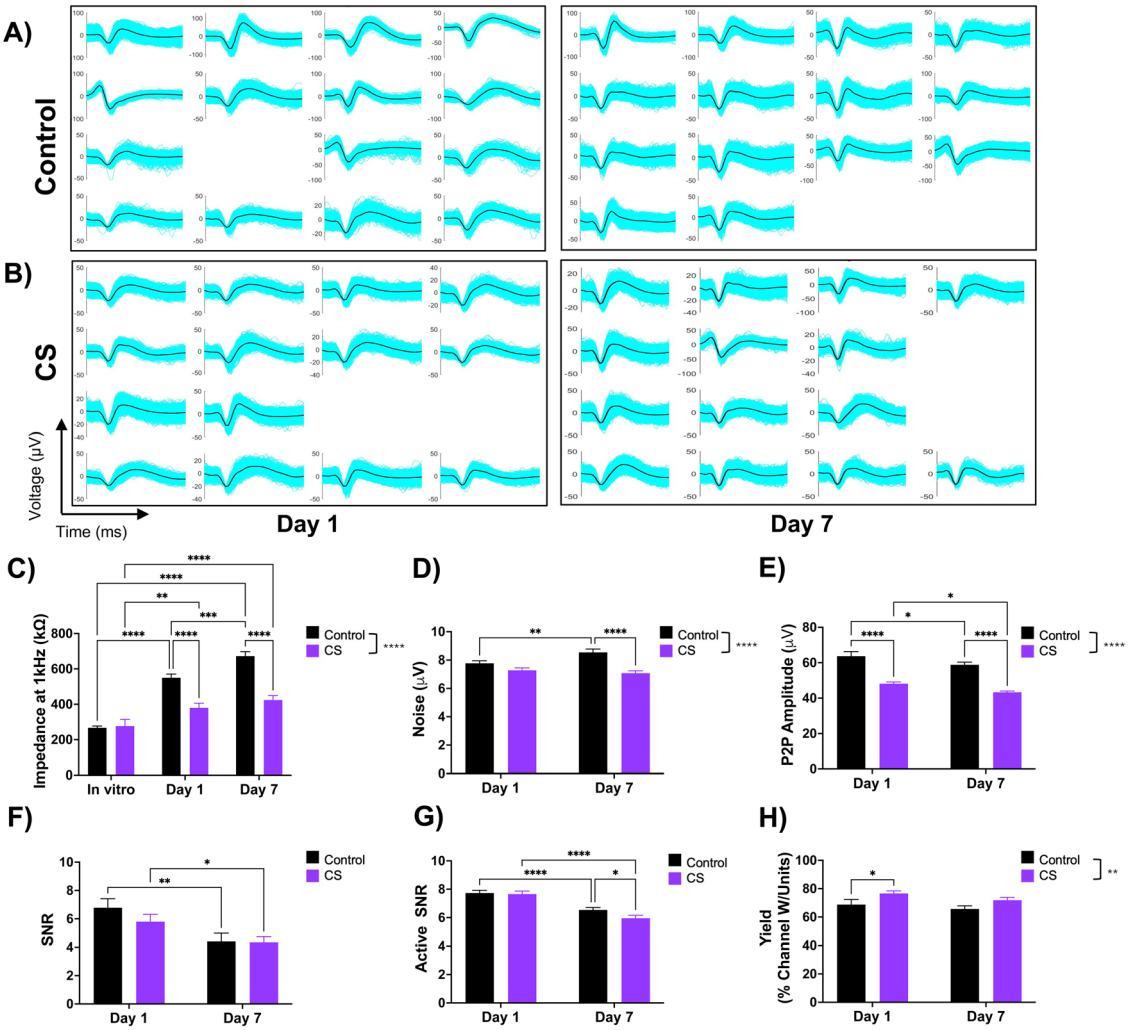


Fig. 7 *In vivo* electrophysiological striatal recording. (A) Single-unit waveforms recorded from a 16-channel silicon electrode from a single animal in the control group ($n$ = 4 per group) at day 1 and day 7. (B) Example waveforms recorded from animals implanted with CS-coated probe ($n$ = 4 animals per group) on day 1 and day 7. Waveforms are plotted in a 1.2 millisecond window. (C) Average impedance measurements for all animals for the control and CS group on day 1 and day 7. (D) Average noise (μV) for all animals. (E) Peak-to-peak amplitude (μV) of the single units recorded from both groups (F) Overall signal-to-noise ratio (SNR) in both groups. (G) Active SNR reporting SNR across channels with sortable single units. (H) Channel yield reporting the % channels recording at least one sortable unit. Group-wise comparisons between different time points are indicated on the figures and overall comparison across all time points is shown next to the legend. Two-way ANOVA with Sidak's multiple comparison tests were used for statistical analysis, $*p < 0.05$, $**p < 0.01$, $***p < 0.001$, $****p < 0.0001$.

surfaces. The hydrophilicity of the surface can reduce the high interfacial energy, making protein adsorption less favorable.[42] This antifouling property is the most valuable during implantation when the surface of the electrode is prone to plasma protein adsorption and inflammatory cell attachment which ultimately dictate the subsequent immune response.[3,46] Thus, the reduction in protein adsorption at this early stage may improve the likelihood of more seamless integration and a dampened chronic immune response.

### 4.2 Bioactivity toward neurons

Primary neurons were cultured on CS-coated substrates to evaluate the coating's specific bioactivity towards neurons. We observed that after 2 days of *in vitro* growth, there were significantly longer neurites on CS-coated substrates as compared to the uncoated bare control. This observation is consistent with other studies that highlighted the neurite-growth-promoting effect of immobilized and highly sulfated sub-types of chondroitin sulfate.[32,47,48] Specifically, one study identified chondroitin sulfate-D as an extracellular ligand for neuronal integrin αVβ3, a heterodimer receptor involved in integrin-mediated cell adhesion pathways.[31] While there are some contradictory *in vitro* findings regarding CS's ability to modulate neuronal growth,[49–51] generally, highly sulfated sub-types have been linked to neuronal growth-promoting properties, whereas lower sulfated sub-types exhibit inhibition towards neuronal growth.[30,52]

As compared to our *in vitro* cell culture studies, we observed a similar effect of the coating on the local neuronal population. We found elevated neuronal nuclei (NeuN) and neurofilament

(NF200) around the coated implant as compared to the control for up to 150 microns from the implant after 1-week of implantation. Interestingly, we observed increased neurofilament expression localized near the coated implant site, potentially suggesting an interaction of the local tissue with the coating.

### 4.3 Effect on acute inflammatory response

Before assessing the inflammatory response to the coating *in vivo*, we cultured primary microglia on CS-coated substrates to better understand the response in a simpler *in vitro* model. We found a significant reduction in the microglial cell viability on CS-coated substrates, which is likely due to the increased hydrophilicity in the coated substrates which prevents microglial adhesion in the first place. Several studies have demonstrated microglial preference towards hydrophobic surfaces for optimal attachment and function.[46,53,54] The reduced cell viability then explains the reduced phagocytic ability, as there are fewer viable cells with limited function. Phagocytosis is a key microglial function that involves clearing out debris from injury or apoptosis and contributes to neuronal network development along with maintaining homeostasis.[55,56] However, during pathological conditions such as chronic inflammation, damaged or stressed, but still viable, neurons may aberrantly get removed by microglia. This heightened phagocytic activity may result in premature neuronal loss and neurodegeneration.[44,57] We observed this phenomenon close to the probe hole in the control group but not in the CS group (ESI,† Fig. S2). Thus, it is possible that the observed reduction in microglial activation and enhancement of neuronal population around the coated probe could be due to fewer abnormal microglia prematurely engulfing neurons. Since electrode implantation is inherently traumatic and induces local inflammation, the coating's dampening effect on the microglial phagocytic response might help with neuronal survival.

Acute histological studies showed a dramatic reduction in the Iba-1 intensity around the CS-coated site as compared to the control. Our *in vitro* studies suggest that surface hydrophilicity of the coated electrodes prevents non-specific protein fouling, which is the initiating step for the acute inflammatory response. Reduction in protein fouling could dampen the microglial migration and activation towards the injury site, supported by the reduced Iba-1 intensity around the coated electrode, as compared to the control (Fig. 6(A) and (B)). Previous work with hydrophilic anti-fouling zwitterionic polymers demonstrated a significantly lower percentage of electrode surface area encapsulated by microglia, as observed with two-photon microscopy.[9,10]

We did not observe any significant differences between astrocytic reactivity around the implant site between the groups, which is likely due to the acute nature of the implantation. The formation of a glial scar, composed of reactive astrocytes, is characteristic of chronic implantation, typically longer than one week.[58] The intensity of IgG protein fouling, an indicator of blood–brain barrier leakage, was significantly lower around the CS-coated implants. The reduction in microglial activation could potentially reduce the BBB damage in the CS group as compared to the control. The anti-fouling property of the surface could further reduce the adsorption of the leaking IgG protein. The higher wettability of the coated probe could also aid in the insertion, providing more lubrication[59] while resisting non-specific protein fouling. Examination of the explanted electrode surface also showed that the CS-coated surface resisted adherence of biological matter as compared to the uncoated probes (ESI,† Fig. S1). Taken with other results that demonstrate the anti-fouling nature of the coating, these observations corroborate the finding.

### 4.4 Effect on recording quality

The increased wettability of CS-coated electrodes likely reduced the *in vitro* electrochemical impedance of the device as compared to the control electrodes. This trend was observed even after *in vivo* implantation (Fig. 7(C)). The hydrophilic coating can not only provide a lubricating surface during insertion,[59] but also prevent non-specific protein adsorption during the initial implantation, further dampening the acute inflammatory response. While not a perfect measure, the electrical impedance can hint at the extent of tissue encapsulation.[60,61] We observed lower impedance sustained throughout implantation in the coated group which indicates lower protein adsorption and glial encapsulation around coated electrodes as compared to the control group.

Overall, we observed similar recording performance between the control and CS groups (Fig. 7(E)–(H)). This is still encouraging and indicates that the coating did not exhibit any toxic or detrimental effects on the nearby tissue. Interestingly, even though the average peak-to-peak amplitude recorded from the coated probes was lower than the control group, it remained relatively stable for the implantation duration for both groups. While the intended implantation region was the same between animals, there is natural variability in the anatomical regions from where the electrodes are recording. Electrode sites that are closer to the axonal regions of the medium spiny neurons, likely pick up smaller amplitude spikes as opposed to the soma, which can generate larger amplitude spikes.[62–64]

We also observed lower noise floor levels for coated electrodes as compared to the control group. Therefore, despite recording lower amplitude single units from the coated electrodes, due to the lower noise floor, the resulting SNR values were ultimately insignificant between the coated and control groups and declined after a week in both groups. The SU yield was overall higher in the CS group as compared to the control group, indicating a higher number of electrode sites actively recording units. Thus, while the coating did not contribute to enhancing the SU amplitude, it helped to enhance the SU yield of the electrodes.

Implantable microelectrode arrays have been used extensively to record extracellular neural activity from various cortical regions[65–69] to better understand underlying neural circuitry and associated behaviors. Compared to the control group in our previous studies,[16,18] with chronic recordings from the cortical regions, in our current study, we observed a slower decline in the impedance, noise floor, and SU yield for

 

the week-long implantation period in the striatum. In terms of biocompatibility, the CS coating demonstrated an overall similar benefit in reducing the tissue response when compared to previously published studies utilizing non-biologic anti-fouling zwitterionic coating[9] and biomimetic L1-coating in mice at the 1-week time point.[70]

Despite the wide range of recording studies, there is a limited understanding of the *in vivo* extracellular single-unit neural electrophysiology of deep brain structures like the amygdala[71] and striatum.[72] These regions are involved in multiple functions including memory, reward, learning, and emotional response, and dysregulated function is implicated in several psychiatric and neurological diseases.[73] In addition to reporting the efficacy of a novel polysaccharide-based coating, this current study also illuminates the extracellular neurophysiological activity of striatal medium spiny neurons, which play a critical role in driving motivated behavior. Future work will explore the coating's effect on the tissue response and neurophysiological recording quality for a chronic implantation period.

## 5. Conclusion

In this work, we investigated the use of a chondroitin sulfate (CS) based coating for neural recording electrodes. The hydrophilic CS coating exhibited a significant reduction in non-specific protein fouling through *in vitro* and *in vivo* studies as compared to uncoated controls. The coating also promoted neurite attachment and outgrowth of primary neurons *in vitro* and an enhanced neuronal population *in vivo*. We observed a reduction in microglia attachment and activation both in our *in vitro* cell culture and *in vivo* histology studies. Lastly, we performed weekly impedance and electrophysiological recordings from CS-coated silicon electrodes implanted in the striatum for 7 days. We observed lower impedance and noise floor from CS-coated devices, and comparable recording performance (channel yield and signal-to-noise ratio) to that recorded from control electrodes. This work highlights the untapped potential of utilizing a novel CS-based coating for improving the biocompatibility of neural electrodes and its application in investigating the understudied striatum electrophysiology.

## Conflicts of interest

There are no conflicts of interest to declare.

## Acknowledgements

This work was funded by the following grants: NIH NINDS BRAIN R01 NS110564, U01NS113279, NIH NIMH R01NG106460 and NIH Bioengineering in Psychiatry Training grant T32 MH119168. We thank the Center for Biological Imaging at the University of Pittsburgh for the confocal microscopy support.

## References

1 A. B. Schwartz, Cortical Neural Prosthetics, *Annu. Rev. Neurosci.*, 2004, **27**, 487–507, DOI: 10.1146/annurev.neuro.27.070203.144233.
2 T. D. Y. Kozai, Z. Du, Z. V. Gugel, M. A. Smith, S. M. Chase, L. M. Bodily, E. M. Caparosa, R. M. Friedlander and X. T. Cui, Comprehensive Chronic Laminar Single-Unit, Multi-Unit, and Local Field Potential Recording Performance with Planar Single Shank Electrode Arrays, *J. Neurosci. Methods*, 2015, **242**, 15–40, DOI: 10.1016/j.jneumeth.2014.12.010.
3 T. D. Y. Kozai, A. S. Jaquins-Gerstl, A. L. Vazquez, A. C. Michael and X. T. Cui, Brain Tissue Responses to Neural Implants Impact Signal Sensitivity and Intervention Strategies, *ACS Chem. Neurosci.*, 2015, **6**(1), 48–67, DOI: 10.1021/cn500256e.
4 T. Saxena, L. Karumbaiah, E. A. Gaupp, R. Patkar, K. Patil, M. Betancur, G. B. Stanley and R. V. Bellamkonda, The Impact of Chronic Blood–Brain Barrier Breach on Intracortical Electrode Function, *Biomaterials*, 2013, **34**(20), 4703–4713, DOI: 10.1016/j.biomaterials.2013.03.007.
5 J. W. Salatino, K. A. Ludwig, T. D. Y. Kozai and E. K. Purcell, Glial Responses to Implanted Electrodes in the Brain, *Nat. Biomed. Eng.*, 2017, **1**(11), 862–877, DOI: 10.1038/s41551-017-0154-1.
6 T. D. Y. Kozai, A. L. Vazquez, C. L. Weaver, S.-G. Kim and X. T. Cui, In Vivo Two-Photon Microscopy Reveals Immediate Microglial Reaction to Implantation of Microelectrode through Extension of Processes, *J. Neural Eng.*, 2012, **9**(6), 066001, DOI: 10.1088/1741-2560/9/6/066001.
7 M. E. Franklin, C. Bennett, M. Arboite, A. Alvarez-Ciara, N. Corrales, J. Verdelus, W. D. Dietrich, R. W. Keane, J. P. de Rivero Vaccari and A. Prasad, Activation of Inflammasomes and Their Effects on Neuroinflammation at the Microelectrode-Tissue Interface in Intracortical Implants, *Biomaterials*, 2023, **297**, 122102, DOI: 10.1016/j.biomaterials.2023.122102.
8 V. S. Polikov, P. A. Tresco and W. M. Reichert, Response of Brain Tissue to Chronically Implanted Neural Electrodes, *J. Neurosci. Methods*, 2005, **148**(1), 1–18, DOI: 10.1016/j.jneumeth.2005.08.015.
9 A. Golabchi, B. Wu, B. Cao, C. J. Bettinger and X. T. Cui, Zwitterionic Polymer/Polydopamine Coating Reduce Acute Inflammatory Tissue Responses to Neural Implants, *Biomaterials*, 2019, **225**, 119519, DOI: 10.1016/j.biomaterials.2019.119519.
10 Q. Yang, B. Wu, J. R. Eles, A. L. Vazquez, T. D. Y. Kozai and X. T. Cui, Zwitterionic Polymer Coating Suppresses Microglial Encapsulation to Neural Implants I*n Vitro* and *In Vivo*, *Adv. Biosyst.*, 2020, 1900287, DOI: 10.1002/adbi.201900287.
11 Q. Li, C. Wen, J. Yang, X. Zhou, Y. Zhu, J. Zheng, G. Cheng, J. Bai, T. Xu, J. Ji, S. Jiang, L. Zhang and P. Zhang, Zwitterionic Biomaterials, *Chem. Rev.*, 2022, **122**(23), 17073–17154, DOI: 10.1021/acs.chemrev.2c00344.
12 C.-H. Lin and S.-C. Luo, Zwitterionic Conducting Polymers: From Molecular Design, Surface Modification, and Interfacial Phenomenon to Biomedical Applications, *Langmuir*, 2022, **38**(24), 7383–7399, DOI: 10.1021/acs.langmuir.2c00448.
13 D. Shi, V. Dhawan and X. T. Cui, Bio-Integrative Design of the Neural Tissue-Device Interface, *Curr. Opin. Biotechnol*, 2021, **72**, 54–61, DOI: 10.1016/j.copbio.2021.10.003.

14 J. E. Collazos-Castro, G. R. Hernández-Labrado, J. L. Polo and C. García-Rama, N-Cadherin- and L1-Functionalised Conducting Polymers for Synergistic Stimulation and Guidance of Neural Cell Growth, *Biomaterials*, 2013, **34**(14), 3603–3617, DOI: 10.1016/j.biomaterials.2013.01.097.

15 R. W. Wiertz, E. Marani and W. L. Rutten, Neural Cell-Cell and Cell-Substrate Adhesion through N-Cadherin, N-CAM and L1, *J. Neural Eng.*, 2011, **8**(4), 046004, DOI: 10.1088/1741-2560/8/4/046004.

16 A. Golabchi, K. M. Woeppel, X. Li, C. F. Lagenaur and X. T. Cui, Neuroadhesive Protein Coating Improves the Chronic Performance of Neuroelectronics in Mouse Brain, *Biosens. Bioelectron.*, 2020, **155**, 112096, DOI: 10.1016/j.bios.2020.112096.

17 J. R. Eles, A. L. Vazquez, N. R. Snyder, C. Lagenaur, M. C. Murphy, T. D. Y. Kozai and X. T. Cui, Neuroadhesive L1 Coating Attenuates Acute Microglial Attachment to Neural Electrodes as Revealed by Live Two-Photon Microscopy, *Biomaterials*, 2017, **113**, 279–292.

18 K. Woeppel, V. Dhawan, D. Shi and X. T. Cui, Nanotopography-Enhanced Biomimetic Coating Maintains Bioactivity after Weeks of Dry Storage and Improves Chronic Neural Recording, *Biomaterials*, 2023, **302**, 122326, DOI: 10.1016/j.biomaterials.2023.122326.

19 G. Li, Y. Liu, Y. Chen, Y. Xia, X. Qi, X. Wan, Y. Jin, J. Liu, Q. He, K. Li and J. Tang, Robust, Self-Adhesive, and Low-Contact Impedance Polyvinyl Alcohol/Polyacrylamide Dual-Network Hydrogel Semidry Electrode for Biopotential Signal Acquisition, *SmartMat*, 2024, **5**(2), e1173, DOI: 10.1002/smm2.1173.

20 Z. Rao, T. Lin, S. Qiu, J. Zhou, S. Liu, S. Chen, T. Wang, X. Liu, Q. Zhu, Y. Bai and D. Quan, Decellularized Nerve Matrix Hydrogel Scaffolds with Longitudinally Oriented and Size-Tunable Microchannels for Peripheral Nerve Regeneration, *Mater. Sci. Eng., C*, 2021, **120**, 111791, DOI: 10.1016/j.msec.2020.111791.

21 K. C. Breen, C. M. Coughlan and F. D. Hayes, The Role of Glycoproteins in Neural Development Function, and Disease, *Mol. Neurobiol.*, 1998, **16**(2), 163–220, DOI: 10.1007/BF02740643.

22 Z. Hu, Q. Niu, B. S. Hsiao, X. Yao and Y. Zhang, Bioactive Polymer-Enabled Conformal Neural Interface and Its Application Strategies, *Mater. Horiz.*, 2023, **10**(3), 808–828, DOI: 10.1039/D2MH01125E.

23 Y. Ando, H. Okada, G. Takemura, K. Suzuki, C. Takada, H. Tomita, R. Zaikokuji, Y. Hotta, N. Miyazaki, H. Yano, I. Muraki, A. Kuroda, H. Fukuda, Y. Kawasaki, H. Okamoto, T. Kawaguchi, T. Watanabe, T. Doi, T. Yoshida, H. Ushikoshi, S. Yoshida and S. Ogura, Brain-Specific Ultrastructure of Capillary Endothelial Glycocalyx and Its Possible Contribution for Blood Brain Barrier, *Sci. Rep.*, 2018, **8**(1), 17523, DOI: 10.1038/s41598-018-35976-2.

24 K. Furukawa, T. Okuda and K. Furukawa, Roles of Glycolipids in the Development and Maintenance of Nervous Tissues, *Methods Enzymol.*, 2006, **417**, 37–52, DOI: 10.1016/S0076-6879(06)17004-4.

25 L. Rao, Y. Liu and H. Zhou, Significantly Improved Cell Affinity of Polydimethylsiloxane Enabled by a Surface-Modified Strategy with Chemical Coupling, *J. Mater. Sci. Mater. Med.*, 2022, **33**(10), 66, DOI: 10.1007/s10856-022-06690-3.

26 V. Dhawan and X. Tracy Cui, Carbohydrate Based Biomaterials for Neural Interface Applications, *J. Mater. Chem. B*, 2022, **10**(25), 4714–4740, DOI: 10.1039/D2TB00584K.

27 S. Avram, S. Shaposhnikov, C. Buiu and M. Mernea, Chondroitin Sulfate Proteoglycans: Structure-Function Relationship with Implication in Neural Development and Brain Disorders, *BioMed Res. Int.*, 2014, **2014**, 642798, DOI: 10.1155/2014/642798.

28 C. I. Gama, S. E. Tully, N. Sotogaku, P. M. Clark, M. Rawat, N. Vaidehi, W. A. Goddard, A. Nishi and L. C. Hsieh-Wilson, Sulfation Patterns of Glycosaminoglycans Encode Molecular Recognition and Activity, *Nat. Chem. Biol.*, 2006, **2**(9), 467–473, DOI: 10.1038/nchembio810.

29 S. Hatano and H. Watanabe, Regulation of Macrophage and Dendritic Cell Function by Chondroitin Sulfate in Innate to Antigen-Specific Adaptive Immunity, *Front. Immunol.*, 2020, 11, DOI: 10.3389/fimmu.2020.00232.

30 C. P. Mencio, R. K. Hussein, P. Yu and H. M. Geller, The Role of Chondroitin Sulfate Proteoglycans in Nervous System Development, *J. Histochem. Cytochem.*, 2021, **69**(1), 61–80, DOI: 10.1369/0022155420959147.

31 M. Shida, T. Mikami, J. I. Tamura and H. Kitagawa, Chondroitin Sulfate-D Promotes Neurite Outgrowth by Acting as an Extracellular Ligand for Neuronal Integrin alphaVbeta3, *Biochim. Biophys. Acta, Gen. Subj.*, 2019, **1863**(9), 1319–1331, DOI: 10.1016/j.bbagen.2019.06.004.

32 A. M. Clement, S. Nadanaka, K. Masayama, C. Mandl, K. Sugahara and A. Faissner, The DSD-1 Carbohydrate Epitope Depends on Sulfation, Correlates with Chondroitin Sulfate D Motifs, and Is Sufficient to Promote Neurite Outgrowth, *J. Biol. Chem.*, 1998, **273**(43), 28444–28453, DOI: 10.1074/jbc.273.43.28444.

33 S. Nadanaka, A. Clement, K. Masayama, A. Faissner and K. Sugahara, Characteristic Hexasaccharide Sequences in Octasaccharides Derived from Shark Cartilage Chondroitin Sulfate D with a Neurite Outgrowth Promoting Activity, *J. Biol. Chem.*, 1998, **273**(6), 3296–3307.

34 F. Cheng, J. Shang and D. M. Ratner, A Versatile Method for Functionalizing Surfaces with Bioactive Glycans, *Bioconjugate Chem.*, 2011, **22**(1), 50–57, DOI: 10.1021/bc1003372.

35 J. van der Vlist, I. Schönen and K. Loos, Utilization of Glycosyltransferases for the Synthesis of a Densely Packed Hyperbranched Polysaccharide Brush Coating as Artificial Glycocalyx, *Biomacromolecules*, 2011, **12**(10), 3728–3732, DOI: 10.1021/bm2009763.

36 K. M. Woeppel, X. S. Zheng and X. T. Cui, Enhancing Surface Immobilization of Bioactive Molecules via a Silica Nanoparticle Based Coating, *J. Mater. Chem. B*, 2018, **6**(19), 3058–3067, DOI: 10.1039/C8TB00408K.

37 M. Pool, J. Thiemann, A. Bar-Or and A. E. Fournier, NeuriteTracer: A Novel ImageJ Plugin for Automated

 

Quantification of Neurite Outgrowth, *J. Neurosci. Methods*, 2008, **168**(1), 134–139, DOI: 10.1016/j.jneumeth.2007.08.029.

38 H. Lian, E. Roy and H. Zheng, Microglial Phagocytosis Assay, *Bio-Protoc.*, 2016, **6**(21), DOI: 10.21769/BioProtoc.1988.

39 B. Wu, E. Castagnola, C. A. McClung and X. T. Cui, PEDOT/CNT Flexible MEAs Reveal New Insights into the Clock Gene's Role in Dopamine Dynamics, *Adv. Sci.*, 2024, 2308212, DOI: 10.1002/advs.202308212.

40 T. D. Y. Kozai, Z. Gugel, X. Li, P. J. Gilgunn, R. Khilwani, O. B. Ozdoganlar, G. K. Fedder, D. J. Weber and X. T. Cui, Chronic Tissue Response to Carboxymethyl Cellulose Based Dissolvable Insertion Needle for Ultra-Small Neural Probes, *Biomaterials*, 2014, **35**(34), 9255–9268.

41 S. Bauer, M. P. Arpa-Sancet, J. A. Finlay, M. E. Callow, J. A. Callow and A. Rosenhahn, Adhesion of Marine Fouling Organisms on Hydrophilic and Amphiphilic Polysaccharides, *Langmuir*, 2013, **29**(12), 4039–4047, DOI: 10.1021/la3038022.

42 B. K. D. Ngo and M. A. Grunlan, Protein Resistant Polymeric Biomaterials, *ACS Macro Lett.*, 2017, **6**(9), 992–1000, DOI: 10.1021/acsmacrolett.7b00448.

43 C. A. Butler, A. S. Popescu, E. J. A. Kitchener, D. H. Allendorf, M. Puigdellívol and G. C. Brown, Microglial Phagocytosis of Neurons in Neurodegeneration, and Its Regulation, *J. Neurochem.*, 2021, **158**(3), 621–639, DOI: 10.1111/jnc.15327.

44 M. Fricker, J. J. Neher, J.-W. Zhao, C. Théry, A. M. Tolkovsky and G. C. Brown, MFG-E8 Mediates Primary Phagocytosis of Viable Neurons during Neuroinflammation, *J. Neurosci.*, 2012, **32**(8), 2657–2666, DOI: 10.1523/JNEUROSCI.4837-11.2012.

45 D. Zhang and G. Nagayama, Effective Wetting Area Based on Electrochemical Impedance Analysis: Hydrophilic Structured Surface, *Langmuir*, 2019, **35**(50), 16508–16513, DOI: 10.1021/acs.langmuir.9b03349.

46 B. K. Leung, R. Biran, C. J. Underwood and P. A. Tresco, Characterization of Microglial Attachment and Cytokine Release on Biomaterials of Differing Surface Chemistry, *Biomaterials*, 2008, **29**(23), 3289–3297, DOI: 10.1016/j.biomaterials.2008.03.045.

47 S. E. Tully, R. Mabon, C. I. Gama, S. M. Tsai, X. Liu and L. C. Hsieh-Wilson, A Chondroitin Sulfate Small Molecule That Stimulates Neuronal Growth, *J. Am. Chem. Soc.*, 2004, **126**(25), 7736–7737, DOI: 10.1021/ja0484045.

48 A. M. Clement, K. Sugahara and A. Faissner, Chondroitin Sulfate E Promotes Neurite Outgrowth of Rat Embryonic Day 18 Hippocampal Neurons, *Neurosci. Lett.*, 1999, **269**(3), 125–128, DOI: 10.1016/S0304-3940(99)00432-2.

49 H. Wang, Y. Katagiri, T. E. McCann, E. Unsworth, P. Goldsmith, Z.-X. Yu, F. Tan, L. Santiago, E. M. Mills, Y. Wang, A. J. Symes and H. M. Geller, Chondroitin-4-Sulfation Negatively Regulates Axonal Guidance and Growth, *J. Cell Sci.*, 2008, **121**(18), 3083–3091, DOI: 10.1242/jcs.032649.

50 L. Karumbaiah, S. Anand, R. Thazhath, Y. Zhong, R. J. Mckeon and R. V. Bellamkonda, Targeted downregulation of N-acetylgalactosamine 4-sulfate 6-O-sulfotransferase significantly mitigates chondroitin sulfate proteoglycan-mediated inhibition, *Glia*, 2011, **59**(6), 981–996, DOI: 10.1002/glia.21170.

51 S. S. Deepa, Y. Umehara, S. Higashiyama, N. Itoh and K. Sugahara, Specific Molecular Interactions of Oversulfated Chondroitin Sulfate E with Various Heparin-Binding Growth Factors. Implications as a Physiological Binding Partner in the Brain and Other Tissues, *J. Biol. Chem.*, 2002, **277**(46), 43707–43716, DOI: 10.1074/jbc.M207105200.

52 P. Yu, C. S. Pearson and H. M. Geller, Flexible Roles for Proteoglycan Sulfation and Receptor Signaling, *Trends Neurosci.*, 2018, **41**(1), 47–61, DOI: 10.1016/j.tins.2017.10.005.

53 E. Park, M. Lee, M. L. S. Poon, E. Lee, S. G. Im and J. H. Shin, Wettability-Based Cell Sorting: Exploring Label-Free Isolation Strategy for Mixed Primary Glial Cell Population, *Adv. Mater. Interfaces*, 2022, **9**(22), 2200388, DOI: 10.1002/admi.202200388.

54 K. Nakajima, S. Honda, Y. Nakamura, F. López-Redondo, S. Kohsaka, M. Yamato, A. Kikuchi and T. Okano, Intact Microglia Are Cultured and Non-Invasively Harvested without Pathological Activation Using a Novel Cultured Cell Recovery Method, *Biomaterials*, 2001, **22**(11), 1213–1223, DOI: 10.1016/S0142-9612(00)00270-2.

55 D. A. Galloway, A. E. M. Phillips, D. R. J. Owen and C. S. Moore, Phagocytosis in the Brain: Homeostasis and Disease, *Front. Immunol.*, 2019, 10.

56 S. A. Wolf, H. W. G. M. Boddeke and H. Kettenmann, Microglia in Physiology and Disease, *Annu. Rev. Physiol.*, 2017, **79**(1), 619–643, DOI: 10.1146/annurev-physiol-022516-034406.

57 T. C. Hornik, A. Vilalta and G. C. Brown, Activated Microglia Cause Reversible Apoptosis of Pheochromocytoma Cells, Inducing Their Cell Death by Phagocytosis, *J. Cell Sci.*, 2016, **129**(1), 65–79, DOI: 10.1242/jcs.174631.

58 R. Biran, D. C. Martin and P. A. Tresco, Neuronal Cell Loss Accompanies the Brain Tissue Response to Chronically Implanted Silicon Microelectrode Arrays, *Exp. Neurol.*, 2005, **195**(1), 115–126, DOI: 10.1016/j.expneurol.2005.04.020.

59 A. Niemczyk, M. El Fray and S. E. Franklin, Friction Behaviour of Hydrophilic Lubricious Coatings for Medical Device Applications, *Tribol. Int.*, 2015, **89**, 54–61, DOI: 10.1016/j.triboint.2015.02.003.

60 W. M. Grill and J. Thomas Mortimer, Electrical Properties of Implant Encapsulation Tissue, *Ann. Biomed. Eng.*, 1994, **22**(1), 23–33, DOI: 10.1007/BF02368219.

61 J. C. Williams, J. A. Hippensteel, J. Dilgen, W. Shain and D. R. Kipke, Complex Impedance Spectroscopy for Monitoring Tissue Responses to Inserted Neural Implants, *J. Neural Eng.*, 2007, **4**(4), 410, DOI: 10.1088/1741-2560/4/4/007.

62 D. A. Henze, Z. Borhegyi, J. Csicsvari, A. Mamiya, K. D. Harris and G. Buzsáki, Intracellular Features Predicted by Extracellular Recordings in the Hippocampus In Vivo, *J. Neurophysiol.*, 2000, **84**(1), 390–400, DOI: 10.1152/jn.2000.84.1.390.

63 A. Kamondi, L. Acsády and G. Buzsáki, Dendritic Spikes Are Enhanced by Cooperative Network Activity in the Intact Hippocampus, *J. Neurosci.*, 1998, **18**(10), 3919–3928, DOI: **10.1523/JNEUROSCI.18-10-03919.1998**.

64 K. H. Pettersen and G. T. Einevoll, Amplitude Variability and Extracellular Low-Pass Filtering of Neuronal Spikes, *Biophys. J.*, 2008, **94**(3), 784–802, DOI: **10.1529/biophysj.107.111179**.

65 D. McCreery, A. Lossinsky, V. Pikov and X. Liu, Microelectrode Array for Chronic Deep-Brain Microstimulation and Recording, *IEEE Trans. Biomed. Eng.*, 2006, **53**(4), 726–737, DOI: **10.1109/TBME.2006.870215**.

66 G. Mendoza, A. Peyrache, J. Gámez, L. Prado, G. Buzsáki and H. Merchant, Recording Extracellular Neural Activity in the Behaving Monkey Using a Semichronic and High-Density Electrode System, *J. Neurophysiol.*, 2016, **116**(2), 563–574, DOI: **10.1152/jn.00116.2016**.

67 B. Brett-Green, E. Fifková, D. T. Larue, J. A. Winer and D. S. Barth, A Multisensory Zone in Rat Parietotemporal Cortex: Intra- and Extracellular Physiology and Thalamocortical Connections, *J. Comp. Neurol.*, 2003, **460**(2), 223–237, DOI: **10.1002/cne.10637**.

68 S. H. Sun, A. Almasi, M. Yunzab, S. Zehra, D. G. Hicks, T. Kameneva, M. R. Ibbotson and H. Meffin, Analysis of Extracellular Spike Waveforms and Associated Receptive Fields of Neurons in Cat Primary Visual Cortex, *J. Physiol.*, 2021, **599**(8), 2211–2238, DOI: **10.1113/JP280844**.

69 R. C. Kelly, M. A. Smith, J. M. Samonds, A. Kohn, A. B. Bonds, J. A. Movshon and T. S. Lee, Comparison of Recordings from Microelectrode Arrays and Single Electrodes in the Visual Cortex, *J. Neurosci.*, 2007, **27**(2), 261–264, DOI: **10.1523/JNEUROSCI.4906-06.2007**.

70 K. M. Woeppel and X. T. Cui, Nanoparticle and Biomolecule Surface Modification Synergistically Increases Neural Electrode Recording Yield and Minimizes Inflammatory Host Response, *Adv. Healthcare Mater.*, 2021, **10**(16), 2002150, DOI: **10.1002/adhm.202002150**.

71 E. Likhtik, J. G. Pelletier, A. T. Popescu and D. Paré, Identification of Basolateral Amygdala Projection Cells and Interneurons Using Extracellular Recordings, *J. Neurophysiol.*, 2006, **96**(6), 3257–3265, DOI: **10.1152/jn.00577.2006**.

72 J. Alegre-Cortés, M. Sáez, R. Montanari and R. Reig, Medium Spiny Neurons Activity Reveals the Discrete Segregation of Mouse Dorsal Striatum, *eLife*, 2021, **10**, e60580, DOI: **10.7554/eLife.60580**.

73 Q. Kong, V. Sacca, M. Zhu, A. K. Ursitti and J. Kong, Anatomical and Functional Connectivity of Critical Deep Brain Structures and Their Potential Clinical Application in Brain Stimulation, *J. Clin. Med.*, 2023, **12**(13), 4426, DOI: **10.3390/jcm12134426**.

 